Effects of Silole Content and Doping on the Electronic Structures and Excitation Energies of Silole/Thiophene Cooligomers

**Guiling Zhang,[†,‡] Jing Ma,*,[†] and Yuansheng Jiang[†]**

Department of Chemistry, Institute of Theoretical and Computational Chemistry, Lab of Mesoscopic Materials Science, Nanjing University, Nanjing, 210093, P. R. China, and Department of Chemistry, Harbin Normal University, Harbin, 150080, P. R. China

ABSTRACT: The effects of siloles and doping with positive and negative charges on the electronic structures and band gaps of the silole/thiophene copolymers are studied employing the density functional theory and the time-dependent density functional theory with B3LYP functional. The optimized geometries, the calculated excitation energies, and the extrapolated band gaps agree with the available experimental results. The decreasing trend of the calculated band gaps with the increasing silole content in the silole/thiophene copolymers is in good agreement with experimental observations. Doping significantly shortens the carbon−carbon distances along the backbones and lowers the excitation energies of thiophene oligomers and silole/thiophene cooligomers relative to those of the neutral ones. Moreover, the low oxidized states have the lower vertical excitation energies than the high oxidized ones. There also exists the even/odd effect in excitation energies of the charged oligomers. The doped copolymers with higher silole content are suggested to be the potential conducting polymers with narrow band gaps. The injected charges by doping lead to the formations of polarons or bipolarons, which are characterized by the distortions in geometries, fluctuations in the bond order waves and spin densities. The even/odd effect in excitation energies is also qualitatively explained by the different widths of subgaps split by the formations of polaron and biopolaron.

1. Introduction

Polythiophene (PT), **1**, has attracted much attention due to their interesting electrical properties and rela-

1 (PT)   **2** (PSi)   **3** (PSiT$_m$) m=1,2,3,4
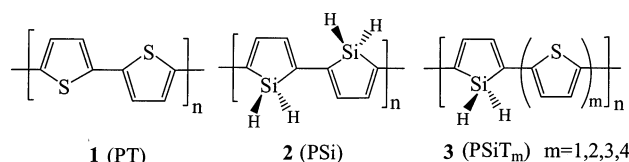
tively higher stability than polypyrrole and polyfuran.[1−3] Accordingly, the modified polymers built on thiophene units have become the focus of achieving novel polymers with small band gaps, E_g. Recently, polysilole (PSi), **2**, was also suggested to be one of potential candidates for its narrower band gap (1.39−1.44 eV by theoretical calculations)[4−6] than that of PT (2.2 eV obtained experimentally).[2] Therefore, it is reasonable to anticipate that the introduction of silole units into the PT chain can lower the band gap and give rise to some interesting materials. Experimental efforts have been devoted to exploring such oligomers and polymers. The derivatives of silole/thiophene copolymers **3** have been synthesized and a decrease in band gaps was observed with the increasing silole content.[7−9] In this theoretical work, we aim to gain an insight into the effects of silole and charge dopings on the electronic structures and properties of silole/thiophene cooligomers **3a−c** in comparison with those of the thiophene oligomers **1** in a systematic way (Figure 1).

Theoretical studies for the better understanding of the electronic properties of polyaromatic oligomers and polymers usually place emphases on their ground-state
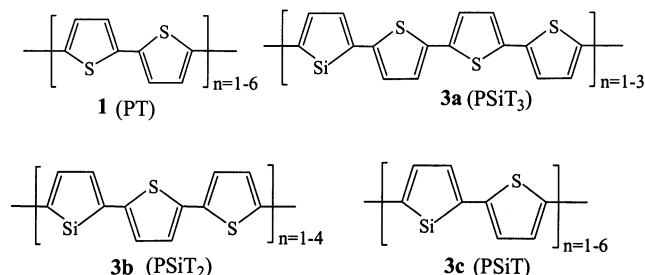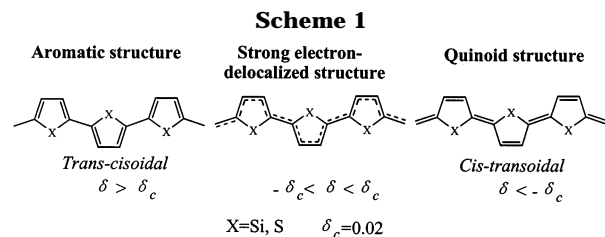
[†] Nanjing University.
[‡] Harbin Normal University.

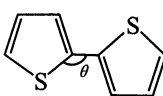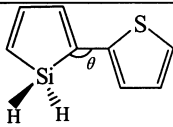**Figure 1.** Structures of the studied oligomers.

Scheme 1

geometries and band gaps. The relationship between the aromatic or quinoid geometry (Scheme 1) of the ground state and the band gap has attracted intensive theoretical studies at various levels,[10−12] which raises a way to design the polymers with small band gaps by modifying the structures toward the quinoid geometries. For example, a quinoid form of a derivative of PT was predicted to possess a near-zero band gap.[13] While in this work, we will show the silole effects by studying how the ground-state geometries of the silole/thiophene cooligomers, **3a−c**, vary with the content of silole rings.

On the other hand, there exist a variety of theoretical approaches for evaluating the band gap of a polymer. One way is based on the ground-state properties, from which the band gap is estimated from the energy difference between the highest occupied molecular

Table 1. Inter-Ring Bond Distance ($r_{\alpha\alpha}$), Average Bond Alternation Parameter ($\bar{\delta}$), Inter-Ring Bond Angle (θ) and Excitation Energies of Bithiophene and Silole/Thiophene Dimer[e]

	$r_{\alpha\alpha}$ /Å	$\bar{\delta}_{inter}$[a]	$\bar{\delta}_{ring}$[b]	$\theta(T)$ /°	$r_{\alpha\alpha}$ /Å	$\bar{\delta}_{inter}$[a]	$\bar{\delta}_{ring}$[b]	$\theta(Si)$ /°
Exptl.[c]	1.456	0.061	0.042	121.9				
3-21G	1.433	0.046	0.046	120.0	1.431	0.046	0.066	120.9
6-31G	1.439	0.046	0.047	120.1	1.436	0.045	0.061	127.6
6-31G*	1.451	0.052	0.037	120.9	1.444	0.052	0.058	127.6
6-31G**	1.450	0.050	0.036	120.9	1.444	0.052	0.058	126.4
6-311G**	1.450	0.052	0.037	120.9	1.443	0.053	0.059	126.4
	Excitation energy by TDDFT /eV							
Exptl.	4.12[d]							
6-31G*	4.02				3.39			
6-31+G*	3.87				3.28			

[a] The average alternation parameters of δ_{inter} over dimers. [b] The average alternation parameters of δ_{ring} over dimers. [c] Reference 28. [d] Reference 29. [e] TDDFT calculations are carried out at the optimized geometry with a B3LYP functional and a 6-31G* basis set. The definition of alternation parameters is shown in Scheme 2.

orbital (HOMO) and the lowest unoccupied molecular orbital (LUMO), termed the HOMO−LUMO gap. Good agreements between the HOMO−LUMO gaps and experimental observations in some polyaromatic polymers have been demonstrated with semiempirical models, ab initio molecular orbital methods and density founctional theory (DFT).[4,14−16] The time-dependent density functional theory (TDDFT), a powerful tool for calculating excitation energies, is also employed to extrapolate band gaps of polymers from the calculated excitation energies of their oligomers.[17−21] It is pointed out that TDDFT systematically underestimated the excitation energies by 0.4−0.7 eV comparing to the experimental results[18,22] due to the limitation of the current approximate exchange-correlation functionals in correctly describing the exchange-correlation potential in the asymptotic region.[23,24] However, reasonable results can still be expected here, because (1) we use the Hartree−Fock (HF)/DFT hybrid functionals such as B3LYP, which could partially overcome the asymptotic problem[17,18] and because (2) we study the homologous silole/thiophene cooligomers, **3a−c**, with our interests in their relative excitation energies to those thiophene oligomers, **1**. So we can probe the relationship between the band gaps and the silole content by the TDDFT/B3LYP calculations on the excitation energies of a sequence of increasing longer thiophene oligomers, **1**, and silole/thiophene cooligomers, **3a−c**, with up to 12 units and by extrapolations of band gaps for their corresponding polymers.

Furthermore, doping is an essential factor in experiments for exploring the conducting materials, since polymers can be semiconductors or even conductors only under doping condition. Different doping styles result in different band gaps of the doped polymers. Therefore, it is also important to analyze the properties of various charge-doped states for guiding experimental efforts toward the exploration of novel polymers with narrow band gaps. However, theoretical studies on the effects of doping on the electronic structures and band gaps are still rare to date. When the chain is doped with the electron-withdrawing (called p-type) or electron-donating (n-type) dopants, the injected charges are viewed as being stored in the form of polaron or bipolaron.[25] The formations of polarons or bipolarons are assumed to be accompanied by the changes in the modes of bond alternation, fluctuations in bond orders, distributions of spin densities, and band gaps, which will be demonstrated in this work.
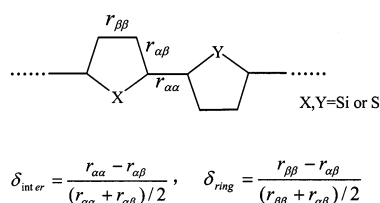
In summary, we try to elucidate (1) the effects of silole content on the geometries and the band gaps of neutral silole/thiophene copolymers and (2) the influence of various charge doping ($n = \pm 1$ to ± 4) on the electronic structures and excitation energies of PT, $\mathbf{1}^{n\pm}$, and silole/thiophene cooligomers, $\mathbf{3a−c}^{n\pm}$ (cf. Figure 1) employing the DFT and TDDFT methods with B3LYP functional in this study.

2. Computational Details

The ground-state geometries of the studied oligomers are fully optimized using DFT with B3LYP functional, as implemented in Gaussian 98[26] on the SGI 3800 workstation. The experiments show that the crystal structures of thiophene oligomers (e.g., the bithiophene, the quaterthiphene, and the sexithiophene) are planar or nearly planar,[1] so we shall restrict ourselves to study the planar structures of oligomers **1** and **3a−c**.

We use bithiophene and silole/thiophene dimer as model substances to test the influence of the basis sets on the optimized geometries (Table 1). As mentioned above, our main interest in the study of the ground-state geometries of oligomers is to see whether they are of aromatic or quinoid geometries, which is able to provide a clear and qualitative picture for experimentalists (cf. Scheme 1). To facilitate the discussion of the

Scheme 2

$$\delta_{inter} = \frac{r_{\alpha\alpha} - r_{\alpha\beta}}{(r_{\alpha\alpha} + r_{\alpha\beta})/2}, \quad \delta_{ring} = \frac{r_{\beta\beta} - r_{\alpha\beta}}{(r_{\beta\beta} + r_{\alpha\beta})/2}$$

difference between the aromatic and quinoid geometries, two bond alternation parameters, δ_{inter} and δ_{ring},[29] are defined as $\delta_{inter} = (r_{\alpha\alpha} - r_{\alpha\beta})/[(r_{\alpha\alpha} + r_{\alpha\beta})/2]$, and $\delta_{ring} = (r_{\beta\beta} - r_{\alpha\beta})/[(r_{\beta\beta} + r_{\alpha\beta})/2]$, respectively, where $r_{\alpha\alpha}$ denotes the inter-ring bond length, and $r_{\alpha\beta}$ and $r_{\beta\beta}$ are the intra-ring bond lengths as being labeled in Scheme 2. In the following sections, we will discuss the geometrical distortions in the backbones of oligomers upon the introduction of silicon atoms and the doping with positive or negative charges on the basis of these two alternation parameters. Therefore, the inter-ring distances and the average bond alternation parameters, $\bar{\delta}_{inter}$ and $\bar{\delta}_{ring}$ for bithiophene and silole/thiophene dimer are listed in Table 1 in comparison with the available experiments. Both the inter-ring distances and the average alternation parameters of bithiophene obtained from the basis of 6-31G* are in good agreement with the experimental data, and they agree within 0.001 Å in $r_{\alpha\alpha}$ and 0.002 in $\bar{\delta}$ with those from the larger basis sets such as 6-31G** and 6-311G**. In addition, the inter-ring bond angle, θ, represented in Table 1 is of interest because it is related to the linearity of the backbone in the long-chain oligomer. From Table 1, we find that optimizations of bithiophene at the basis sets of 6-31G*, 6-31G**, and 6-311G** yield the identical value of $\theta = 120.9°$, reproducing the experimental result ($\theta = 121.9°$). Thus, the basis set of 6-31G* is employed in the geometry optimizations for the thiophene oligomers and silole/thiophene cooligomers with up to 12 units.

TDDFT calculations of the vertical excitation energies are then performed at the optimized geometries of the ground states. Table 1 also lists the excitation energies of bithiophene and silole/thiophene dimer using the basis sets of both the 6-31G* and 6-31+G* at the optimized geometry with the 6-31G* basis set. The excitation energy of bithiophene obtained from TDDFT/6-31G* is close to the experiment value with the variance of 0.10 eV. However, for the unknown silole/thiophene dimer, the TDDFT excitation energy calculated at the 6-31G* basis set is only slightly different from that obtained at the basis set of 6-31+G*. Moreover, we are interested in the relative excitation energies of silole/thiophene oligomers (**3a**–**c**) to those of oligothiophenes (**1**) and the relative excitation energies of doped oligomers ($\mathbf{1}^{n\pm}$ and $\mathbf{3a}$–$\mathbf{c}^{n\pm}$) to those of the undoped ones (**1** and **3a**–**c**). Therefore, the basis set of 6-31G* is utilized in all TDDFT calculations for the sake of the easier convergence in computations for the longer cooligomers containing siloles. Band gaps of silole/thiophene copolymers with various silole content are also estimated by plotting the vertical excitation energies for the first dipole-allowed excited states of cooligomers against the reciprocal chain lengths and extrapolating to infinite chain length.

For the charge-doped oligomers $\mathbf{1}^{n\pm}$ and $\mathbf{3a}$–$\mathbf{c}^{n\pm}$, we studied the low-lying states for all possible spin multiplicities by the unrestricted DFT calculations and

Table 2. Optimized Geometries of Oligomers 1 and 3a–c[a]

oligomer	$\bar{r}_{\alpha\alpha}$/Å	$\bar{\delta}_{inter}$	$\bar{\delta}_{ring}$(T)	$\bar{\delta}_{ring}$(Si)	$\bar{\theta}$(Si)/deg
1	1.442	0.036	0.030		
3a	1.438	0.034	0.025	0.056	126.6
3b	1.436	0.030	0.021	0.055	126.6
3c	1.433	0.029	0.019	0.053	126.7

[a] $\bar{r}_{\alpha\alpha}$ is the average inter-ring bond distance, $\bar{\delta}_{inter}$ is the average inter-ring bond alternation parameter, $\bar{\delta}_{ring}$(T) and $\bar{\delta}_{ring}$(Si) are the average intra-ring bond alternation parameters over thiophene rings and silole rings, respectively, and $\bar{\theta}$(Si) is the average inter-ring bond angle expanded by the inter-ring bond and intra-carbon–silicon bond.

further evaluated the lowest excitation energies at the ground-state structures by TDDFT calculations.

3. Results and Discussions

3.1. Silole Effects on Neutral Polymers. Theoretical investigations of influences of silole units on the ground-state geometries, HOMO–LUMO gaps, and excitation energies of the silole/thiophene cooligomers are carried out using the DFT and TDDFT methods.

Geometry. From Table 1, we can notice that the introduction of silole in silole/thiophene dimer does lead to some changes in the geometry: the inter-ring bond distance $r_{\alpha\alpha}$ is shortened, the average intra-ring alternation parameters, $\bar{\delta}_{ring}$ is magnified, and the inter-ring bond angle (θ) is enlarged relative to those of the bithiophene. Now, the longer oligomers containing 12 rings, **1** and **3a**–**c**, are selected to elucidate the effects of silole content on the ground-state geometries (Figure 1). The optimized configurations of oligomers are presented in Figure 2. Calculation results of the average inter-ring bond distances, $\bar{r}_{\alpha\alpha}$, the average inter-ring bond alternation parameters, $\bar{\delta}_{inter}$, the average intra-ring bond alternation parameters, $\bar{\delta}_{ring}$(T) and $\bar{\delta}_{ring}$(Si) over the thiophene and silole rings, respectively, and the average inter-ring bond angle, $\bar{\theta}$, are listed in Table 2.

At the first glance, it is interesting to notice that in **3a** and **3c**, where the silole and thiophene units are odd-alternatively aligned in the ratio of 1:3 and 1:1, respectively, all the silicon atoms appear on the same side of the backbones of oligomers and their structures tend to be bending in the boatlike shape with the increase in the silole content. The inter-ring bond angle, θ may give us a clue to understand such deviations from the linear backbones in these cooligomers. In fact, there is little difference in θ between the dimers and the longer oligomers (cf. Tables 1 and 2). Clearly, the inter-ring bond angle (θ) is enlarged by the introduction of siloles. Thus, the distortions of the backbones are amplified by the larger θ stretching in the same directions perpendicular to the chain axes with the increasing silole content from **3a** to **3c**. In contrast, in **3b**, where the silole units are bridged with two thiophene units (in the ratio of 1:2), the larger inter-ring bond angles stretch out in the opposite directions from the backbone, and consequently the global structure of backbone differs only slightly from that of duodecithiophene (**1**).

Then a closer look into geometries of silole/thiophene cooligomers, **3a**–**c** in comparison with that of duodecithiophene (**1**) is taken from the average inter-ring bond length, $\bar{r}_{\alpha\alpha}$, as shown in Table 2. The values of $\bar{r}_{\alpha\alpha}$ in oligomers **1** and **3a**–**c** exhibit a decreasing trend with the increasing ratio of silole/thiophene (cf. Table 2), implying that the introduction of siloles induces the gradual change toward the more quinoid structure.
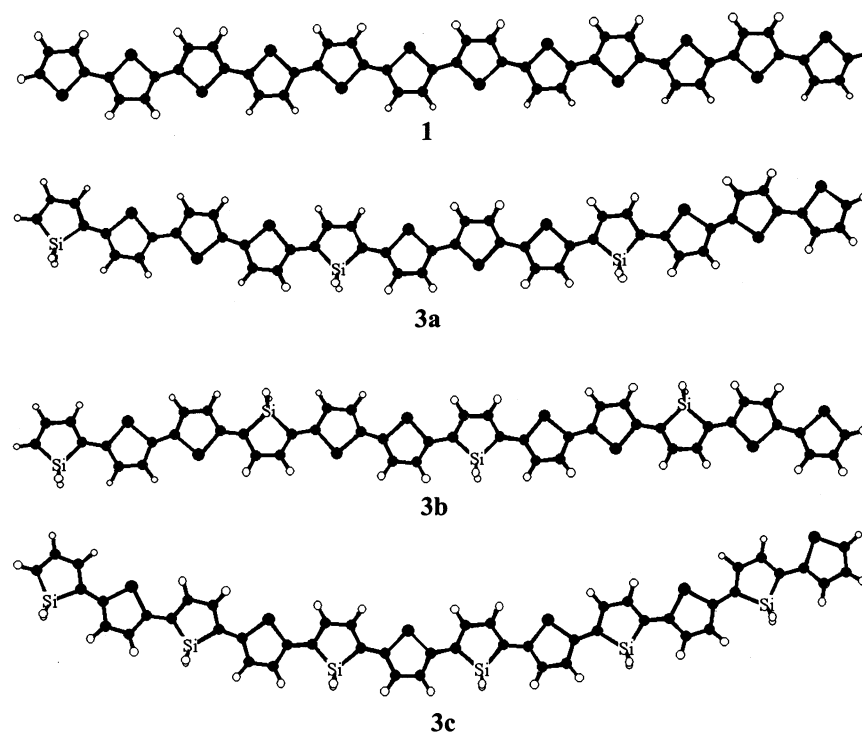
Figure 2. Optimized configurations of oligothiophene (**1**) and silole/thiophene cooligomers (**3a**−**c**) with 12 rings. The silicon atoms are labeled out to distinguish between the silole and thiophene units.
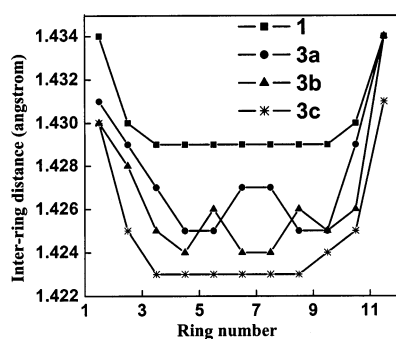

Figure 3. Variation of inter-ring distances over the neutral oligomer chains.

Moreover, the effect of siloles on the contractions of the $r_{\alpha\alpha}$ can be more directly perceived from Figure 3, where the inter-ring bond distances along the chains of **1** and **3a**−**c** are depicted. In view of the increasingly quinoid structures from **3a** to **3c**, the reductions in the band gaps of silole/thiophene copolymers with the increase in the silole content can be anticipated, which will be confirmed by our TDDFT calculations in the following subsection.

The average inter- and intra-ring bond alternation parameters, $\bar{\delta}_{inter}$ and $\bar{\delta}_{ring}$ in Table 2 may also furnish useful information relevant to the structures of oligomers, **1** and **3a**−**c**. When some thiophene rings are replaced by silole rings in **3a**−**c**, changes in the alternation parameters are mainly reflected in the $\bar{\delta}_{ring}$ rather than in the $\bar{\delta}_{inter}$ (cf. Table 2). So, we will concentrate on the results of $\bar{\delta}_{ring}$ to understand the silole effects on the geometries of the individual silole and thiophene rings, respectively. It is found that silole units impact two influences on the ring geometries. One effect is that the extent of bond alternations over thiophene rings in silole/thiophene cooligomers (**3a**−**c**) becomes smaller. It is reflected by the smaller $\bar{\delta}_{ring}(T)$ (less than 0.025) in

3a−**c** than that of the duodecithiophene (**1**) ($\bar{\delta}_{ring}(T) = 0.030$). Another effect is that the structures of silole units tend to have larger bond alternations than those of thiophene rings ($\bar{\delta}_{ring}(Si) > 0.053$). Therefore, the introduction of silicon atoms gives rise to the local geometrical distortions along the backbones of cooligomers, making it possible to form the conjugational defects and to lower the band gaps of the silole/thiophene copolymers.

Band Gaps. The TDDFT excitation energies and HOMO−LUMO gaps of oligomers **1** and **3a**−**c** as well as the extrapolated band gaps for the corresponding polymers are listed in Table 3. Similar to our previous work on the other oligomers,[17] we obtain the linear correlations among TDDFT band gaps, HOMO−LUMO band gaps, and experimental results as exhibited in Figure 4. The extrapolated band gaps from the TDDFT excitation energies and HOMO−LUMO gaps slightly underestimate the excitation energies by the average values of 0.45 and 0.28 eV, respectively, comparing to the available experimental data. Two factors may be responsible for deviations from experiments. One is that there exist systematical underestimations by 0.4−0.7 eV inherent in TDDFT calculations as mentioned in the Introduction. Another is that the predicted band gaps are for the isolated gas-phase chains, while the experimental band gaps are measured in the liquid phase where the environmental influence and the interchain interactions may be involved. To achieve more quantitative predictions on the lowest excitation energies by partially alleviating the systematic errors, we introduce an empirical correction with the working function of $E_{corrected} = 0.088E_{TDDFT} + 0.651$, which is obtained by the linear relationship between the experimental values and TDDFT excitation energies (cf. Figure 4). The corrected excitation energies are in better agreement with the experimental data with the average deviation of 0.09 eV.

Table 3. TDDFT Excitation Energies, the Empirically Corrected Excitation Energies, and HOMO−LUMO Gaps, Δ_{H-L}, of Oligomers with B3LYP Functional and 6-31G* Basis Set[e]

oligomer	TDDFT excitation energies/eV	corrected excitation energies/eV	Δ_{H-L}/eV	exptl/eV
PT (**1**)				
$n = 1$	4.02	4.19	4.23	4.12[a]
$n = 2$	2.84	3.15	3.03	
$n = 3$	2.38	2.75	2.61	2.92[b]
$n = 4$	2.15	2.55	2.42	
$n = 5$	2.01	2.42	2.31	
$n = 6$	1.93	2.35	2.24	
$n = \infty$	1.53	2.00	1.85	2.20[c]
PSiT$_3$ (**3a**)				
$n = 1$	2.63	2.97	2.80	
$n = 2$	1.89	2.32	2.11	
$n = 3$	1.65	2.10	1.91	
$n = \infty$	1.33	1.82	1.46	1.83[d]
PSiT$_2$ (**3b**)				
$n = 1$	2.93	3.23	3.09	
$n = 2$	2.06	2.47	2.23	
$n = 3$	1.73	2.18	1.95	
$n = 4$	1.57	2.03	1.82	
$n = \infty$	1.31	1.81	1.54	1.76[d]
PSiT (**3c**)				
$n = 1$	3.39	3.64	3.63	
$n = 2$	2.38	2.75	2.50	
$n = 3$	1.93	2.35	2.07	
$n = 4$	1.68	2.13	1.84	
$n = 5$	1.52	1.99	1.71	
$n = 6$	1.42	1.90	1.63	
$n = \infty$	1.09	1.61	1.25	1.55[c]

[a] Reference 29. [b] Reference 30. [c] Reference 2. [d] Reference 8. [e] The experimental data are given for comparison.
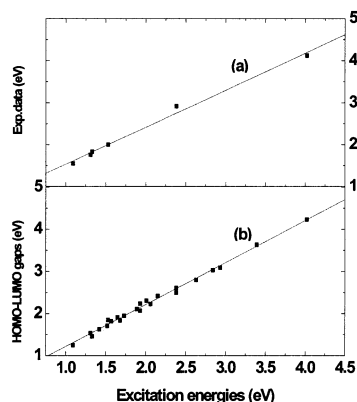

Figure 4. Correlations of TDDFT excitation energies with (a) the experimental data and (b) the HOMO−LUMO gaps.

It is worthwhile to notice in Table 3 that with the increase in the silole content, the band gaps of copolymers become increasingly narrower, i.e., the excitation energies decrease in the order **3a** > **3b** > **3c**. Interestingly, Figure 5 exhibits a linear relationship between the ratio of silole/thiophene and the excitation energies of copolymers, which agrees with the experimental observations.[8]

3.2. Charge-Doping Effects on Oligomers. As already mentioned before, one of the most important features of the π-conjugated polymers is their ability to become highly conducting after oxidative (p-type) or reductive (n-type) doping. The changes in the UV/visible/ near-IR spectrum of thiophene oligomers up to 12 units with increasing oxidation levels have been detected by extensive experimental studies.[30] But less is known
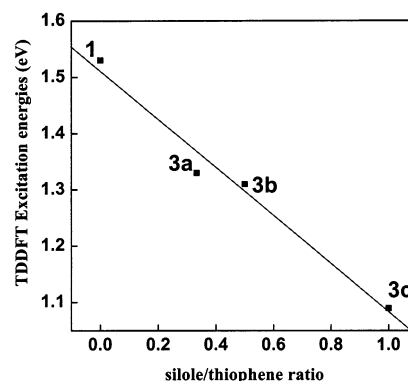

Figure 5. Change in band gaps obtained from TDDFT calculations with the increasing silole/thiophene ratio for a series of cooligomers.

about the doping effects on silole/thiophene cooligomers. To gain a better understanding of the doping influence, theoretical studies of changes in geometries, π bond orders, spin densities along the chain, and excitation energies of cooligomers upon p- and n-doping are carried out on the basis of DFT and TDDFT computations.

Spin Multiplicity. The doping with the even and odd number charges may affect the preference of the spin multiplicities of the ground states. When oligomers doped with the even number charges, $\mathbf{1}^{n\pm}$ and $\mathbf{3a}-\mathbf{c}^{n\pm}$ ($n = 2$ and 4), the ground states may be singlet or triplet, depending on their radical characters.[31] The relative energies with different spin multiplicities of various even-charge doped oligomers to the lowest singlet states are obtained from the unrestricted DFT calculations with the results given in Table 4. The singlet states of PT^{2+} (denoted as $\mathbf{1}^{2+}$) and PT^{2-} ($\mathbf{1}^{2-}$) lie above the triplet ones by 0.098 and 0.054 eV, respectively, suggesting biradical characters with two unpaired electrons in them.[31] However, for the other doped oligomers with the even number of charges, the singlet ground states are preferred. Similarly, Table 5 gives the relative energies of quartet states to the doublet states of the odd-charge doped oligomers, $\mathbf{1}^{n\pm}$ and $\mathbf{3a}-\mathbf{c}^{n\pm}$ ($n = 1$ and 3), showing the preference of the doublet ground states. It is also interesting to compare the energy differences between the states with higher spin multiplicity and that with the lowest spin multiplicity (i.e., $\Delta E = E$ (higher spin multiplicity) $- E$ (the lowest spin multiplicity)) along with the increments in the silole content (cf. Tables 4 and 5). We can find that for both p- and n-dopings, the silole units enlarge the energy differencesΔE in the order of $\mathbf{1}^{n\pm} < \mathbf{3a}^{n\pm} < \mathbf{3b}^{n\pm} < \mathbf{3c}^{n\pm}$, implying that the addition of siloles enhances the preference of the ground state with the lowest spin multiplicity.

Excitation Energies of the Doped Oligomers. Table 6 summarizes the excitation energies of the first optically allowed states obtained from TDDFT calculations, from which three general trends can be found. First, the doping significantly lowers the excitation energies of $\mathbf{1}^{n\pm}$ and $\mathbf{3a}-\mathbf{c}^{n\pm}$ ($n = 1-4$) by around 2 to 4 times relative to those of neutral oligomers **1** and **3a**− **c**, which is consistent with the well-recognized experimental fact that the higher conductivity is achieved upon doping.[32,33] The calculated excitation energies of the doped $\mathbf{1}^{n\pm}$ also agree with experimental UV/vis values.[30] Second, the low-oxidative-doped oligomers have the lower vertical excitation energies than the high-oxidative-doped ones, for instances, $\mathbf{1}^{+}$(0.509 eV) < $\mathbf{1}^{3+}$(0.610 eV) and $\mathbf{3c}^{+}$(0.502 eV) < $\mathbf{3c}^{3+}$(0.610 eV).

Table 4. Relative Energies with Different Spin Multiplicities of Various Even Charged Oligomers to the Lowest Singlet States (E_S), Where $\Delta E_{T-S} = E(\text{triplet}) - E(\text{singlet})$, and $\Delta E_{Q-S} = E(\text{quintet}) - E(\text{singlet})^a$

oligomer	E_S/au	ΔE_{T-S}/eV	$\langle S^2\rangle$	oligomer	E_S/au	ΔE_{T-S}/eV	ΔE_{Q-S}/eV	$\langle S^2\rangle$
				p-Doping				
1^{2+}	−6622.4808	−0.098	2.05	1^{4+}	−6621.7728	0.123	0.769	0.06
$3a^{2+}$	−6299.9677	0.011	0.27	$3a^{4+}$	−6299.2697	0.158	0.787	0.08
$3b^{2+}$	−6192.4674	0.054	0.23	$3b^{4+}$	−6191.7738	0.215	0.912	0.05
$3c^{2+}$	−5977.4669	0.166	0.05	$3c^{4+}$	−5976.7771	0.221	0.991	0.14
				n-Doping				
1^{2-}	−6623.0009	−0.054	2.05	1^{4-}	−6622.8198	0.006	0.026	0.05
$3a^{2-}$	−6300.5002	0.016	0.17	$3a^{4-}$	−6300.3431	0.007	0.028	0.04
$3b^{2-}$	−6193.0025	0.076	0.09	$3b^{4-}$	−6192.8514	0.008	0.029	0.01
$3c^{2-}$	−5978.0073	0.185	0.12	$3c^{4-}$	−5977.8646	0.008	0.035	0.05

^{a} The expectation values of S^2, $\langle S^2\rangle$, are presented to evaluate the spin contaminations.

Table 5. Relative Energies of Quartet States to the Doublet States (E_D) of the Odd Charged Oligomers, Where $\Delta E_{Q-D} = E(\text{quartet}) - E(\text{doublet})^a$

oligomer	E_D/au	$\langle S^2\rangle$	oligomer	E_D/au	ΔE_{Q-D}/eV	$\langle S^2\rangle$
			p-Doping			
1^+	−6622.7354	0.78	1^{3+}	−6622.1612	0.291	1.28
$3a^+$	−6300.2208	0.83	$3a^{3+}$	−6299.6547	0.400	1.23
$3b^+$	−6192.7177	0.83	$3b^{3+}$	−6192.1558	0.414	1.17
$3c^+$	−5977.7116	0.99	$3c^{3+}$	−5977.1561	0.485	1.12
			n-Doping			
1^-	−6622.9957	0.79	1^{3-}	−6622.9436	0.310	1.20
$3a^-$	−6300.4869	0.81	$3a^{3-}$	−6300.4558	0.384	1.23
$3b^-$	−6192.9849	0.81	$3b^{3-}$	−6192.9609	0.405	1.17
$3c^-$	−5977.9812	0.95	$3c^{3-}$	−5977.9687	0.493	1.15

^{a} The expectation values of S^2, $\langle S^2\rangle$, are presented to evaluate the spin contaminations.

Table 6. TDDFT Excitation Energies of the Doped Oligomers, $1^{n\pm}$, 3A-c$^{n\pm}$ (n=1−4)

oligomer	excitation energies /eV	exptl/eV	oligomer	excitation energies/eV	exptl/eV
		p-Doping			
1^+	0.509	0.59^a	1^{3+}	0.610	
$3a^+$	0.525		$3a^{3+}$	0.623	
$3b^+$	0.521		$3b^{3+}$	0.613	
$3c^+$	0.502		$3c^{3+}$	0.610	
1^{2+}	0.673	0.75^a	1^{4+}	0.843	1.18^a
$3a^{2+}$	0.941		$3a^{4+}$	1.003	
$3b^{2+}$	0.971		$3b^{4+}$	1.019	
$3c^{2+}$	1.011		$3c^{4+}$	1.020	
		n-Doping			
1^-	0.513	0.513	1^{3-}	0.571	0.571
$3a^-$	0.522	0.522	$3a^{3-}$	0.579	0.579
$3b^-$	0.518	0.518	$3b^{3-}$	0.574	0.574
$3c^-$	0.507	0.507	$3c^{3-}$	0.570	0.570
1^{2-}	0.640	0.640	1^{4-}	0.951	0.951
$3a^{2-}$	0.895	0.895	$3a^{4-}$	0.892	0.892
$3b^{2-}$	0.930	0.930	$3b^{4-}$	0.950	0.950
$3c^{2-}$	0.975	0.975	$3c^{4-}$	0.964	0.964

^{a} Reference 30.

The third trend is that there exists the even/odd effect in the vertical excitation energies of the charged oligomers. The excitation energies of the odd-charge-doped oligomers are lower than those of the even-charge-doped ones, for examples, 1^+(0.509 eV) < 1^{2+}(0.673 eV) and $3c^+$(0.502 eV) < $3c^{2+}$(1.011 eV). Furthermore, there is also an even/odd effect of silole rings on the excitation energies of the doped cooligomers. The addition of the silole units favors the lower excitation energies for the odd-charged-doped cooligomers, i.e., the excitation energies decrease on the order of $3a^{n\pm}>3b^{n\pm}>3c^{n\pm}$ (n = 1 and 3). When the ratio of silole/thiophene reaches 1:1, $3c^\pm$, the excitation energies are slightly lower than those of $1^\pm$, recommending an alternative candidate to the
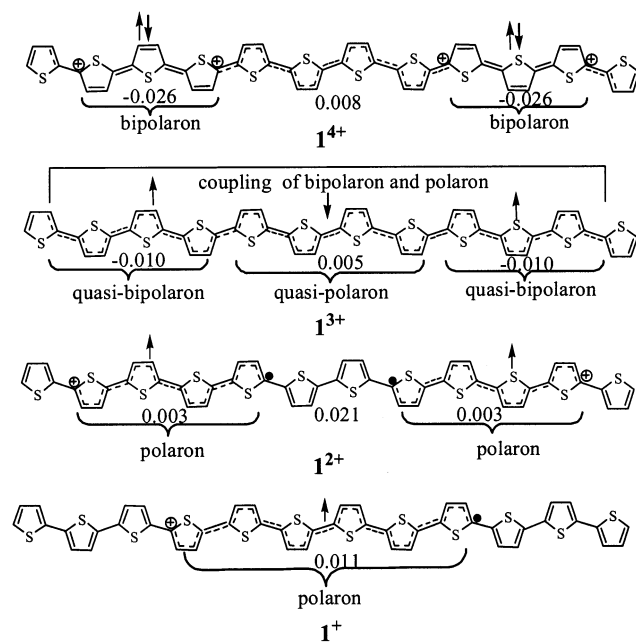

Figure 6. Schematic skeleton of the p-doped 1^{n+}(n = 1−4) with the average values of δ over the characteristic blocks shown below the corresponding regions. Polarons and bipolarons bear positive charge and their representations are referred to ref 1. The up and down arrows denote the radical centers with the α and β spins, respectively.

conducting polymers. But for the even-charge doped cooligomers, the excitation energies increase with the increasing silole content (cf. Table 6). The even/odd effect in the excitation energies of the doped oligomers can be further qualitatively understood from the distributions of the charged polarons and bipolarons and the corresponding changes in orbital levels, which will be discussed as follows.

Polaron and Bipolaron: Understanding from the Geometry, Bond Order, and Spin Density. In this part, two typical oligomers, $1^{n\pm}$ and $3c^{n\pm}$, are taken to illustrate the effects of the doping on distortions in geometries, fluctuations of the π bond orders and the spin densities along the oligomer chains. The features of polaron and bipolaron can be identified by the extent of bond alternations and the distribution of spin densities from the chemical viewpoint as well as fluctuations in the bond-order wave of π electrons from the language of solid-state physics.[34] To gain a comprehensive understanding of the doping effects on **1** and **3c**, the variations in bond alternations, bond-order waves of π electrons, spin densities, and the consequently proposed distributions of polaron or bipolaron in $1^{n\pm}$ and $3c^{n\pm}$ are plotted in Figures 6−13.
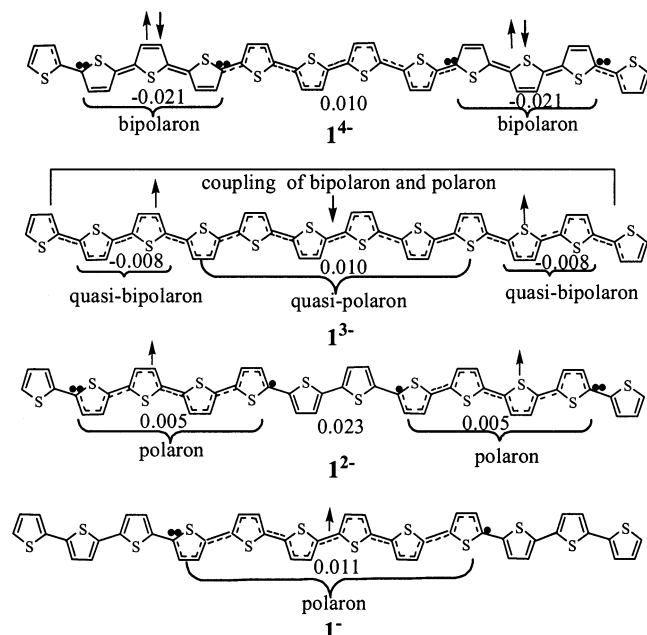
Figure 7. Schematic skeleton of the n-doped 1^{n-} ($n = 1-4$) with the average values of δ over the characteristic blocks shown below the corresponding regions. Polarons and bipolarons bear negative charge and their representations (as double dots) are referred to ref 1. The up and down arrows denote the radical centers with the α and β spins, respectively.
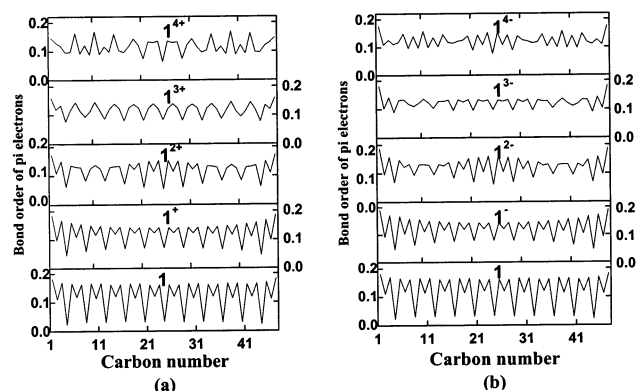

Figure 8. Fluctuations in the bond orders of π electrons along the oligomer chains of (a) 1^{n+} and (b) 1^{n-} ($n = 1-4$) relative to the neutral oligomer **1**.
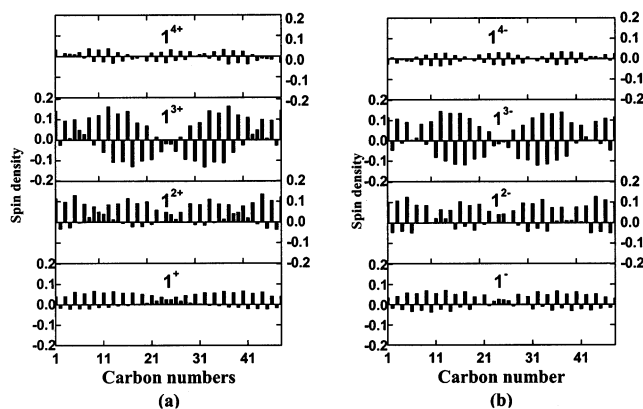

Figure 9. Spin density distributions of carbon atoms along the oligomer chains of the (a) p-doped 1^{n+} and (b) n-doped 1^{n-} ($n = 1-4$).

There is little difference in the optimized configurations of ground states between the doped oligomers, $1^{n\pm}$ and $3c^{n\pm}$ ($n = 1-4$), and the neutral counterparts as
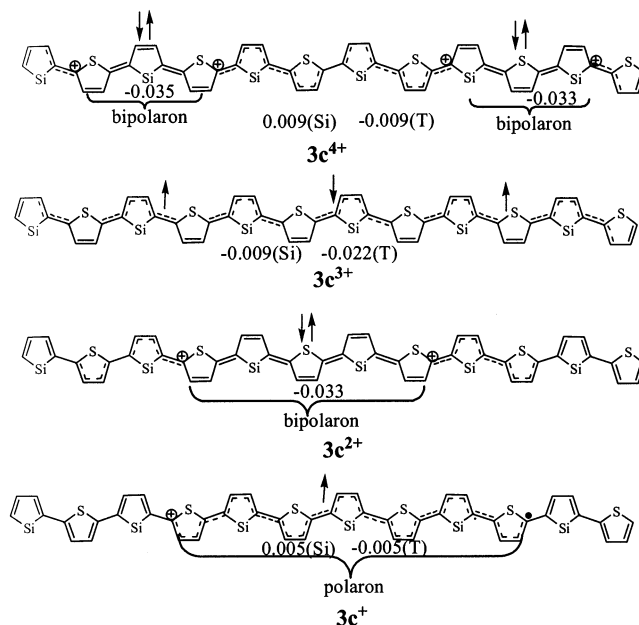

Figure 10. Schematic skeleton of the p-doped $3c^{n+}$ ($n = 1-4$) with the average values of δ over the characteristic blocks shown below the corresponding regions. Polarons and bipolarons bear positive charges, and their representations are referred to ref 1. The up and down arrows denote the radical centers with the α and β spins, respectively.
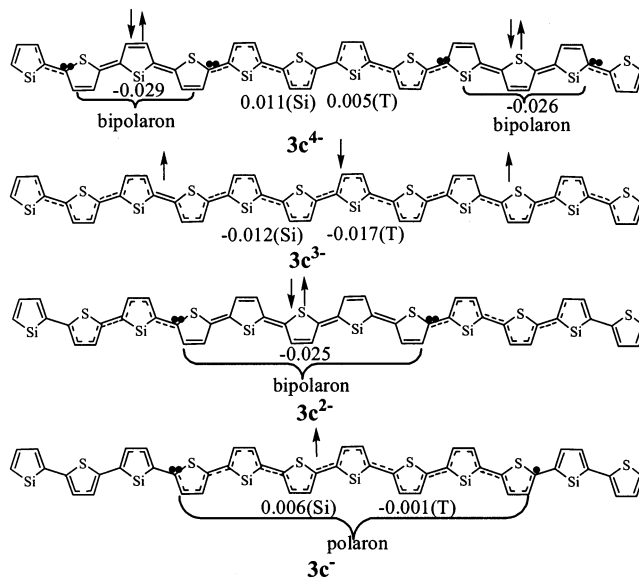

Figure 11. Schematic skeleton of the n-doped $3c^{n-}$ ($n = 1-4$) with the average values of δ over the characteristic blocks shown below the corresponding regions. Polarons and bipolarons bear negative charges, and their representations (as double dots) are referred to ref 1. The up and down arrows denote the radical centers with the α and β spins, respectively.

already depicted in Figure 2. The notable difference lies in significant reductions in distances of both single and double bonds of the C—C skeleton upon p- and n-dopings. For instance, the average C—C bond length in p-doped 1^{4+} is calculated to be 0.032 Å smaller compare to that in **1**. While for the n-doped 1^{4-}, similar reduction of 0.033 Å in the average C—C bond length is also observed. In addition, the calculated values of the average bond alternation parameter, $\bar{\delta}$, for the neutral and the doped thiophene oligomers are given in Table 7. The doped oligomers, $1^{n\pm}$, display a remarkable decrease in the extent of bond alternations by the
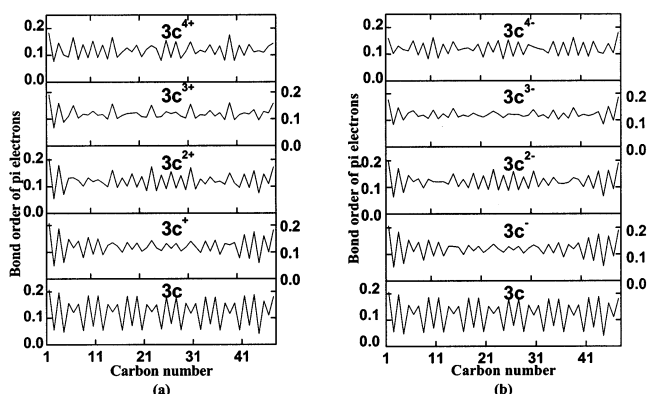
Figure 12. Fluctuations in the bond orders of π electrons along the oligomer chains of (a) $3c^{n+}$ and (b) $3c^{n-}$ ($n = 1-4$) relative to the neutral oligomer $3c$.
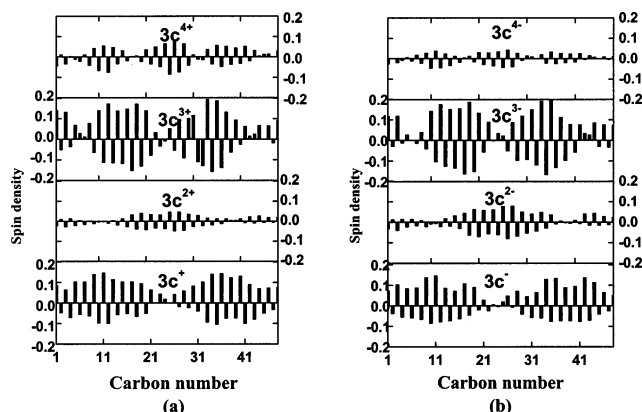
Figure 13. Spin density distributions of carbon atoms along the oligomer chains of the (a) p-doped $3c^{n+}$ and (b) n-doped $3c^{n-}$ ($n = 1-4$).

Table 7. Average Values of Bond Alternation Paramers, $\bar{\delta}$, over the Whole Chains in the Neutral 1 and Doped $1^{n\pm}$ ($n = 1-4$)

oligomer	$\bar{\delta}$	oligomer	$\bar{\delta}$
1	0.033		
1^+	0.018	1^-	0.020
1^{2+}	0.011	1^{2-}	0.015
1^{3+}	0.008	1^{3-}	0.007
1^{4+}	0.016	1^{4-}	0.014

comparison of $\bar{\delta}$ over the whole chain with the neutral oligomer, **1** (cf. Table 7), revealing the tendency toward the more electron-delocalization in global backbones upon both p- and n-dopings. Thus, the mobility of electrons is increased in the doped oligomers, which is in agreement with the appreciable conductivity of 2000 S cm^{-1} of p-doped PT.[32]

The appearance of polaron or bipolaron in the doped chain is known to cause the distortions in the backbone of *trans*-polyacetylene, called the conjugational defects by solid-state physics,[34] where the bond alternation parameter δ changes its sign and there is also a phase jump of 180° in the bond order wave of π electrons. While with the involvement of heteroatoms (sulfur and silicon atoms), the variations in the electronic structures of $1^{n\pm}$ and $3c^{n\pm}$ (n = 1-4) become more complicated than that of the *trans*-polyacetylene. Therefore, it is more convenient for chemists to describe the existence of polaron or bipolaron by the transformation from the local aromatic structure to either the strong electron-delocalized structure or the quinoid structure. The polaron may belong to the former and the bipolaron

belongs to the latter as demonstrated by the experiments[30] and our following discussions. The abrupt changes in the bond lengths, bond order waves of π electrons, and spin densities at the edge of each polaron or bipolaron can be observed in the doped oligomers, from which we draw the possible distributions of the polarons and bipolarons in $1^{n\pm}$ (Figures 6 and 7) and $3c^{n\pm}$ (Figures 10 and 11), respectively.

The bond alternation parameter is helpful to analyze the distortions in geometries of the doped oligomers. The polaron is experimentally detected to spread over five thiophene rings in 1^+,[30] so we define the critical conjugation index, δ_c, of 0.02 to qualitatively assign the aromatic structure, the strong electron-delocalized structure, and the quinoid structure according to the calculated δ_{inter} at the edge of the region of polaron in 1^+ (i.e., δ_c equals δ_{inter} obtained from the begining of the forth ring as referred to Figure 6). Given this definition, when $\delta < -\delta_c$, the local geometry is assumed to be the quinoid structure; the region with $-\delta_c < \delta < \delta_c$ corresponds to the strong electron-delocalizd structure with nearly equal bond lengths, and the case of $\delta > \delta_c$ is called the aromatic structure (Scheme 1). Obviously, the smaller the absolute value of δ is, the stronger delocalization of π electrons appears. Then, on the basis of the critical conjugation index ($\delta_c = 0.02$) and the calculated values of δ for $1^{n\pm}$ and $3c^{n\pm}$, we can easily classify the oligomer backbones into three kinds of the characteristic blocks, i.e., the aromatic and quinoid structures denoted by the alternating single and double bonds and the strong electron-delocalized structure described by the dashed lines (cf. Figures 6, 7, 10, and 11). The values of $\bar{\delta}$ over the characteristic blocks are listed in Figures 6, 7, 10, and 11 below the corresponding regions.

A closer look into the geometrical distortions, characterized by bond alternation parameter δ, is desired to further recognize the distributions of the charged polarons and bipolarons in the doped oligomers. It can be seen from Figures 6 and 7 that in the lower oxidized and reduced thiophene oligomers like $1^\pm$ and $1^{2\pm}$, the polarons appear with the strong electron-delocalized structures (i.e., the requirement of $-\delta_c < \bar{\delta} < \delta_c$ is satisfied in these regions). The single polaron spread from the chain center gradually to two sides of $1^\pm$. On going to $1^{2\pm}$, the structures in Figures 6 and 7 depict a pair of polarons diffusing as apart as possible to the termini of the limited chains due to the Coulomb repulsion of two like charges. However, for the high oxidized and reduced thiophene oligomers, 1^{4+} and 1^{4-}, a pair of bipolarons exists in the form of strong quinoid structures with $\bar{\delta} < -\delta_c$. Similar to the polaron pairs in $1^{2\pm}$, two bipolarons in 1^{4+} and 1^{4-} are also far apart from each other by the Coulomb repulsion. An obvious difference between the $1^{2\pm}$ and $1^{4\pm}$ lies in that the electrons are strongly bounded to the two ends of the $1^{4\pm}$ by bipolarons, and between the pair of bipolarons a region of strong electron-delocalization appears ($\bar{\delta}$ for the central parts are 0.008 in 1^{4+} and 0.010 in 1^{4-}, respectively), indicating the gradually transformation from the quiniod to the aromatic structures via a delocalized region in $1^{4\pm}$. However, for $1^{3\pm}$ the values of $\bar{\delta}$ over different characteristic regions are comparable to each other because of the strong couplings between the polaron and bipolaron. It is not easy to distinguish the boundary between them. We tentatively term those characteristic regions as quasi-polaron and quasi-bipolaron based on the sign of $\bar{\delta}$ (Figures 6 and 7).

The fluctuations of the π bond orders along the oligomer chains in $\mathbf{1}^{n\pm}$ ($n = 1-4$) are also compared with the neutral oligomer $\mathbf{1}$ in Figure 8, which is helpful to further visualize the distributions of the polarons and bipolarons. We can easily see the conjugational defects in the bond order waves of π electrons, where the periodical peaks in the neutral oligomer $\mathbf{1}$ disappear (or say there are phase jumps of 180° from the language of solid-state physicist). The fluctuations of the bond order waves in the p-doped oligomers (Figure 8a) are similiar to those in the n-doped ones (Figure 8b) except that in $\mathbf{1}^{3\pm}$. It is clearly shown in Figure 8 that $\mathbf{1}^{3-}$ has more obvious conjugational defects than $\mathbf{1}^{3+}$, implying the stronger delocalization of π electrons in $\mathbf{1}^{3-}$. This is supported by the lower excitation energy in $\mathbf{1}^{3-}$ (0.571 eV) than that in $\mathbf{1}^{3+}$ (0.610 eV) from TDDFT calculations (cf. Table 6).

On the other hand, the positively and negatively charged polarons according to the condensed matter physics terminology essentially correspond to the radical cation and radical anion in the chemical language.[30] The radical properties of the characteristic regions in the doped oligomers can be reflected by distributions of the spin densities. Figure 9 plots the fluctuations in spin densities of carbon atoms along the oligomer chains $\mathbf{1}^{n\pm}$ ($n = 1-4$), from which we denote the radical centers on the schematic skeletons in Figures 6 and 7 by the up and down arrows representing the α and β spins, respectively. At this point, the physical pictures of the doping effects on the distributions of polarons and bipolarons in PT ($\mathbf{1}$) become clear from the multiple view angles of distortions in geometries and fluctuations in the bond order waves as well as the radical properties.

The doped cooligomers $\mathbf{3c}^{n\pm}$, with $n = 1-4$, exhibit quite different features from $\mathbf{1}^{n\pm}$ owing to the introduction of silole rings. Similar theoretical analyses on $\mathbf{3c}^{n\pm}$ from the distortions in geometries (cf. Figures 10 and 11), the fluctuations in the π bond order waves (Figure 12) and spin densities (Figure 13) have been performed. At first, we investigate the doping effects with the odd number of charges in $\mathbf{3c}^{n\pm}$ ($n = 1,3$). Obviously, in both $\mathbf{3c}^+$ and $\mathbf{3c}^-$, values of $\bar{\delta}$ approach zero (Figures 10 and 11) and the fluctuations of π bond orders are much flatter (cf. Figure 12) than those in $\mathbf{1}^{\pm}$. In other words, the polarons in the middle of $\mathbf{3c}^{\pm}$ have more evident conjugational defects. Consequently, $\mathbf{3c}^+$ is expected to have a smaller band gap than $\mathbf{1}^+$, which is also supported by TDDFT excitation energies (Table 6). Going to the higher oxidative states, all the silole rings in $\mathbf{3c}^{3+}$ present strong electron-delocalized structure with $\bar{\delta}$ of -0.009, while all the thiophene rings favor the quinoid structures with $\bar{\delta}$ of -0.022 (Figure 10). Different from this, in $\mathbf{3c}^{3-}$ the thiophene rings tend to be less quinoid and turn to have the properties of electron-delocalization ($\bar{\delta} = -0.017$). Therefore, the electrons in $\mathbf{3c}^{3-}$ are more delocalized than those in $\mathbf{3c}^{3+}$. This is in agreement with the lower TDDFT excitation energies in $\mathbf{3c}^{3-}$ (0.570 eV) than that in $\mathbf{3c}^{3+}$ (0.610 eV) as listed in Table 6.

Then we continue to study the properties of the doped cooligomers $\mathbf{3c}^{n\pm}$ with the even number of charges ($n = 2,4$). In Figures 10 and 11, the bipolarons appear in the center of $\mathbf{3c}^{2\pm}$ with the strong quinoid structures (in $\mathbf{3c}^{2+}$, $\bar{\delta} = -0.033$; in $\mathbf{3c}^{2-}$, $\bar{\delta} = -0.025$), which is in contrast with two separating polarons in $\mathbf{1}^{2\pm}$ (cf. Figures 6 and 7). This is in agreement with our predictions from the unrestricted DFT calculations that $\mathbf{3c}^{2\pm}$ and $\mathbf{1}^{2\pm}$ are in preference of the singlet and triplet ground states,

Scheme 3

Neutral oligomer   Singly charged (Radical cation)   Doubly charged (Dication)
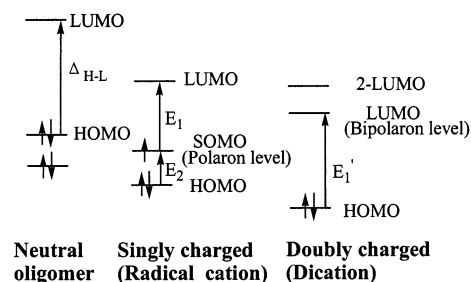
respectively (cf. Table 4). At the higher doping levels, the quinoid structures of bipolarons in $\mathbf{3c}^{4\pm}$ are remarkably strengthened by the addition of silole rings with the more negative values of $\bar{\delta}$ (cf. Figures 10 and 11) than those in $\mathbf{1}^{4\pm}$ (cf. Figures 6 and 7). Therefore, the oxidation and reduction with the even charges cause electrons more localized in the cooligomers, which can be also seen from the large fluctuations in π-electron bond order waves (Figure 12).

To summarize the above discussions, we notice that π electrons are more delocalized in the doped cooligomers with the odd number of charges, $\mathbf{3c}^{n\pm}$ ($n = 1$ and 3), while the electrons are more localized in the even charged $\mathbf{3c}^{n\pm}$ ($n = 2$ and 4) comparing to $\mathbf{1}^{n\pm}$. In other words, the characteristic properties of the polaron and bipolaron are both enhanced by siloles in the doped $\mathbf{3c}^{n\pm}$: the enhanced polarons in the odd oxidized or reduced states are beneficial to the delocalization of π electrons while the enhanced bipolarons prefer the π electron localization in the even oxidized or reduced states. In fact, the even/odd effect in the geometrical distortions characterized by the polarons or bipolarons is closely related to the even/odd effect in excitation energies of the doped oligomers.

Understanding of the Even/Odd Effect from the Orbital Levels. Scheme 3 depicts the energy diagram and the relevant optical transitions of the neutral and charged oligomers, where HOMO, SOMO, and LUMO, 2-LUMO denote the highest occupied molecular orbital (MO), and singly (or spin) occupied MO, lowest unoccupied MO, and second-lowest unoccupied MO, respectively. In a neutral oligomer, the optical transition comes from the HOMO−LUMO transition as displayed in Scheme 3. First, we consider the behavior of a singly oxidized oligomer. When a positive charge is injected into a neutral oligomer (in other words, an electron is removed from it), a SOMO (also called polaron level physically[30]) is formed in the radical cation. The SOMO lies between the HOMO and LUMO, splitting the HOMO−LUMO band into two subgaps (Scheme 3). The dipole-allowed transitions from SOMO to LUMO (E_1) and from the HOMO to SOMO (E_2) can be observed in the subgap region. Our TDDFT calculations on $\mathbf{1}^+$ and $\mathbf{3c}^+$ show that the lowest dipole-allowed transitions mainly correspond to excitations of E_1 with larger transition probabilities than those of E_2. Clearly, the SOMO and LUMO levels come closer with the gap of E_1 compared to Δ_{H-L} in the neutral oligomer. Next, we consider a doubly oxidized oligomer (dication) with an electronic configuration that corresponds to a bipolaron. When another electron is further removed from SOMO of the radical cation, the lowest empty bipolaron level, namely, LUMO, is formed, which leads to the smaller HOMO−LUMO gap of E_1' in the doubly charged oligo-
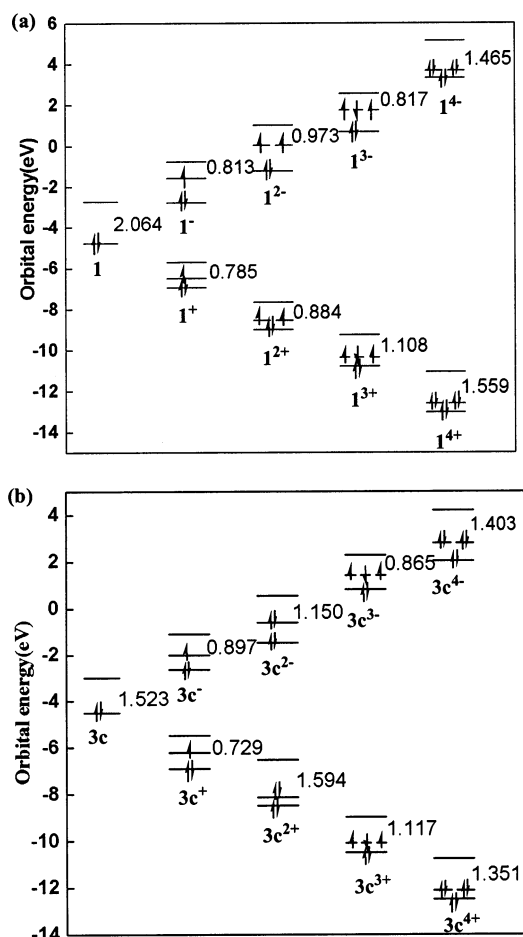
Figure 14. Orbital levels with energy gaps of E_1 (or E_1') of the charged $1^{n\pm}$ and $3c^{n\pm}$ ($n = 1-4$).

mer than the $\Delta_{\text{H-L}}$ in the neutral one (Scheme 3). Therefore, the formations of polarons and bipolarons by the charge doping can lower the band gap of a polymer. In the dication, the transition energy of E_1' becomes greater than the E_1 for the radical cation because of the larger geometrical deformation caused by introducing two charges.[35] To understand the even/odd effect in the excitation energies, we schematically sketch the orbital levels of the charged $1^{n\pm}$ and $3c^{n\pm}$ in Figure 14. We also present the energy gaps of E_1 (or E_1') for all the doped oligomers, from which the even/odd effect in E_1 (or E_1') is easily found (cf. Figure 14). Therefore, the origin of the even/odd effect in excitation energies of the doped oligomers is the different widths of subgaps split by the formations of polaron and bipolaron.

4. Conclusions

The effects of siloles and doping on the electronic structures and band gaps of the silole/thiophene copolymers are investigated employing the density functional theory with B3LYP functional. According to the optimized geometries, the trend toward the stronger quinoid structure with the increasing ratio of silole/thiophene is shown for the neutral cooligomers **3a−c**. Excitation energies of the neutral oligomers **1** and **3a−c** are evaluated by TDDFT. There exits a linear relationship between the TDDFT excitation energies and the experimental values. The corrected excitation energies obtained from this linear correlation agree well with the available experiments. The experimental observation of the inverse proportion between the silole content and

band gaps is well reproduced by our TDDFT calculations.

The doping effects on the excitation energies of oligomers **1** and **3c** can be summarized as follows. First, the doping can remarkably contract the carbon−carbon bond distances and lower the excitation energies of $1^{n\pm}$ and $3c^{n\pm}$ by around 2−4 times relative to the neutral ones. Second, the low oxidized states have the lower vertical excitation energies than the high oxidized ones. Third, the even/odd effect in the vertical excitation energies of the doped oligomers is discovered.

The polarons and bipolarons formed by the charge doping can be well identified from the distortions in geometries, fluctuations in bond-order waves of π electrons and spin densities. The characteristic structure of the polaron shows more delocalization of π electron than that of the bipolaron. The introduction of siloles strengthens both the polaron properties and the bipolaron properties in the doped cooligomers: the enhanced polarons in the odd oxidized or reduced states are beneficial to the delocalization of π electrons, while the enhanced bipolarons prefer the localization of π electrons in the even oxidized or reduced states. The even/odd effect in the geometrical distortions caused by polarons or bipolarons corresponds to the even/odd effect in the excitation energies of the charged oligomers, which is qualitatively explained by the different widths of subgaps split by the formations of polaron and biopolaron.

Therefore, the doped copolymers with higher silole content are suggested to be the potential conducting polymers with narrow band gaps. Further works toward the exploration of other novel oligomers with some interesting electric properties are still underway.

References and Notes

(1) Kertesz, M. In *Handbook of Organic Conductive Molecules and Polymers*; Nalwa, H. S., Ed.; John Wiley & Sons Ltd.: New York, 1997; Vol. 4, pp147−172.
(2) Roncali, J. *Chem. Rev.* **1997**, *97*, 173−205.
(3) Hong, S. Y.; Marynick, D. S. *J. Chem. Phys.* **1992**, *96*, 5497.
(4) Salzner, U.; Lagowski, J. B.; Pickup, P. G.; Poirier, R. A. *Synth. Met.* **1998**, *96*, 177−189.
(5) Frapper, G.; Kertesz, M. *Synth. Met.* **1993**, *55−57*, 4255−4259.
(6) Frapper, G.; Kertesz, M. *Organometallics.* **1992**, *11*, 3128.
(7) Yamaguchi, S.; Tamao, K. *J. Chem. Soc., Dalton Trans.* **1998**, 3693.
(8) Tamao, K.; Yamaguchi, S.; Goto, T. *Chem. Commu..* **2000**, *39*, 1695.
(9) Tamao, K.; Yamaguchi, S.; Ito, Y.; Matsuzaki, Y.; Yamabe, T.; Fukushima, M.; Mori, S. *Macromolecules.* **1995**, *28*, 8668.
(10) Hong, S. Y.; Marynick, D. S. *Macromolecules.* **1992**, *25*, 4652−4657.
(11) Lee, Y.; Kertesz, M. *J. Chem. Phys.* **1988**, *88*, 2609.
(12) Brédas, J. L. *J. Chem. Phys.* **1985**, *82*, 3808.
(13) Brédas, J. L. *Synth. Met.* **1987**, *17*, 115.
(14) Salzner, U. *Synth. Met.* **2001**, *119*, 215−216.
(15) De Oliveira, M. A.; Duarte, H. A.; Pernaut, J.; De Almeida, W. B. *J. Phys. Chem. A* **2000**, *104*, 8256−8262.
(16) Alexander, O. *J. Chem. Phys.* **1997** *107*, 18, 7331−7344.
(17) (a) Ma, J.; Li, S.; Jiang, Y. *Macromolecules.* **2002**, *35*, 1109−1115. (b) Gao, Y.; Liu, C.; Jiang, Y. *J. Phys. Chem. A* **2002**, *106*, 5380−5384.
(18) Hsu, C.; Hirata, S.; Martin, H. *J. Phys. Chem. A* **2001**, *105*, 451−458.
(19) Kwon, O.; Mckee, M. *J. Phys. Chem.* A **2000**, *104*, 7106−7112.

(20) Hirata, S.; Martin, H. *Chem. Phys. Lett.* **1999**, *302*, 375−382.
(21) Wiberg, K. B.; Stratmann, R. E.; Frisch, M. J. *Chem. Phys. Lett.* **1998**, *297*, 60−64.
(22) Cai, Z.; Sendt, K.; Reimers, J. R. *J. Chem. Phys.* **2002**, *117*, 5543−5549.
(23) Tozer, D. J.; Handy, N. C. *J. Chem. Phys.* **1998**, *109*, 10180.
(24) Casida, M. E.; Jamorski, C.; Casida, K. C.; Salahub, D. R. *J. Chem. Phys.* **1998**, *108*, 4439.
(25) Brédas, J. L.; Cornil, J.; Beljonne, D.; Dos Santos, D. A.; Shuai, Z. *Acc. Chem. Res.* **1999**, *32*, 267−276.
(26) Gaussian 98, Revision A.9. Frisch, M. J.; Trucks, G. W.; Schlegel, H. B.; Scuseria, G. E.; Robb, M. A.; Cheeseman, J. R.; Zakrzewski, V. G.; Montgomery, J. A., Jr.; Stratmann, R. E.; Burant, J. C.; Dapprich, S.; Millam, J. M.; Daniels, A. D.; Kudin, K. N.; Strain, M. C.; Farkas, O.; Tomasi, J.; Barone, V.; Cossi, M.; Cammi, R.; Mennucci, B.; Pomelli, C.; Adamo, C.; Clifford, S.; Ochterski, J.; Petersson, G. A.; Ayala, P. Y.; Cui, Q.; Morokuma, K.; Malick, D. K.; Rabuck, A. D.; Raghavachari, K.; Foresman, J. B.; Cioslowski, J.; Ortiz, J. V.; Stefanov, B. B.; Liu, G.; Liashenko, A.; Piskorz, P.; Komaromi, I.; Gomperts, R.; Martin, R. L.; Fox, D. J.; Keith, T.; Al-Laham, M. A.; Peng, C. Y.; Nanayakkara, A.; Gonzalez, C.; Challacombe, M.; Gill, P. M. W.; Johnson, B. G.; Chen, W.; Wong, M. W.; Andres, J. L.; Head-Gordon, M.; Replogle, E. S.; Pople, J. A. Gaussian, Inc.: Pittsburgh, PA, 1998.

(27) Samdal, S.; Samuelsen, E. J.; Volden, H. V. *Synth. Met.* **1993**, *59*, 259−65.
(28) Brédas, J. L.; Silbey, R.; Boudreaux, D. S.; Chance, R. R. *J. Am. Chem. Soc.* **1983**, *105*, 6555−6559.
(29) Yannoni, C. S.; Clarke, T. C. *Phys. Rev. Lett.* **1983**, *51*, 1191.
(30) Van Haare, J. A. E. H.; Havinga, E. E.; Van Dongen, J. L. J.; Janssen, R. A. J.; Cornil, J.; Brédas, J. L. *Chem.−Eur. J.* **1998**, *4*, 1509−1522.
(31) The radical character with the unpaired electrons is essentially corresponding to the concept of the polaron from the language of solid-state physics.
(32) Roncali, J.; Yassar, A.; Garnier, F. *J. Chem. Soc., Chem. Commun.* **1988**, 581.
(33) McCullough, R. D.; Williams, S. P.; Tristram-Nagle, S.; Jayaraman, M.; Ewbank, P. C.; Miller, L. *Synth. Met.* **1995**, *69*, 279.
(34) Kertesz, M. In *Handbook of Organic Conductive Molecules and Polymers*; Nalwa, H. S., Ed.; John Wiley & Sons Ltd.: New York, 1997; Vol. *2*, pp 14−16.
(35) The negatively charged oligomers also form the SOMO (polaron) levels or the bipolaron levels. Similar discussions on the even/odd effect in the subgaps of E_1 and E_1' of the negatively charged oligomers can be also achieved.